

Comments from Reviewer 2

MINOR COMMENTS

- Line 68-78: Somewhere in this literature review, you should discuss McCreight et al. (2014), which is of high relevance to the current study (e.g., same study area, also uses Lidar data to examine uncertainty from sparse point measurements).

Response: *Thank you, the discussion and reference have been included.*

TECHNICAL COMMENTS/CORRECTIONS

- Line 82: Add “an” before “approach”.

RE: *Corrected.*

- Lines 202-245: This has become an incredibly long paragraph. Please break into two (or more) paragraphs. It may be natural to begin a new paragraph at “Firstly” (line 218), and then another new paragraph at “Secondly” (line 237).

RE: *Thank you. We split the paragraph as suggested.*

- Line 245: Replace “Additionally” with “In addition to”. (“Additionally is an adverb and it does not appear to be appropriate in this context).

RE: *Corrected.*

- Line 508: Add “of” after “case”.

RE: *Corrected.*

- Supplement, Page 4, Line 2: Replace “tem” with “term”.

RE: *Corrected.*

REFERENCES

McCreight, J. L., A. G. Slater, H. P. Marshall, and B. Rajagopalan, 2014: Inference and uncertainty of snow depth spatial distribution at the kilometre scale in the Colorado Rocky Mountains: the effects of sample size, random sampling, predictor quality, and validation procedures. *Hydrol. Process.*, 28, 933–957, doi:10.1002/hyp.9618.

1
2
3
4
5
6
7
8
9
10
11
12
13
14
15
16
17
18
19
20

**THEORETICAL ANALYSIS OF ERRORS WHEN ESTIMATING SNOW DISTRIBUTION
THROUGH POINT MEASUREMENTS**

By

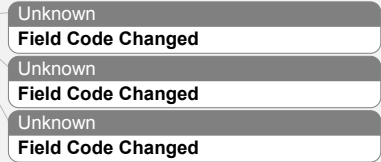
Ernesto Trujillo^{1,2} and Michael Lehning^{2, 1}

1. School of Architecture, Civil and Environmental Engineering, École Polytechnique Fédérale
de Lausanne, Lausanne, Switzerland

2. WSL Institute for Snow and Avalanche Research SLF, Davos, Switzerland

Corresponding Author:

Ernesto Trujillo
EPFL ENAC IIE CRYOS, Station 2
Lausanne, Switzerland, CH-1015
Email: Ernesto.Trujillo@epfl.ch
Office: +41 21 693 5938



Unknown
Field Code Changed

Unknown
Field Code Changed

Unknown
Field Code Changed

21 **Abstract**

22 In recent years, marked improvements in our knowledge of the statistical properties of the
23 spatial distribution of snow properties have been achieved thanks to improvements in measuring
24 technologies (e.g., LIDAR, TLS, and GPR). Despite this objective and quantitative frameworks
25 for the evaluation of errors in snow measurements have been lacking. Here, we present a
26 theoretical framework for quantitative evaluations of the uncertainty in average snow depth
27 derived from point measurements over a profile section or an area. The error is defined as the
28 expected value of the squared difference between the real mean of the profile/field and the
29 sample mean from a limited number of measurements. The model is tested for one and two
30 dimensional survey designs that range from a single measurement to an increasing number of
31 regularly-spaced measurements. Using high-resolution (~ 1m) LIDAR snow depths at two
32 locations in Colorado, we show that the sample errors follow the theoretical behavior.
33 Furthermore, we show how the determination of the spatial location of the measurements can be
34 reduced to an optimization problem for the case of the predefined number of measurements, or to
35 the designation of an acceptable uncertainty level to determine the total number of regularly-
36 spaced measurements required to achieve such error. On this basis, a series of figures are
37 presented as an aid for snow survey design under the conditions described, and under the
38 assumption of prior knowledge of the spatial covariance/correlation properties. With this
39 methodology, better objective survey designs can be accomplished that are tailored to the
40 specific applications for which the measurements are going to be used. The theoretical
41 framework can be extended to other spatially distributed snow variables (e.g., SWE) whose
42 statistical properties are comparable to those of snow depth.

Ernesto 12/5/2015 09:32
Deleted: of
Ernesto 12/5/2015 09:32
Deleted: ,
Ernesto 12/5/2015 09:38
Deleted: and extrapolations
Ernesto 12/5/2015 09:39
Deleted: of point measurements of
Ernesto 12/5/2015 09:39
Deleted: when used to represent the average depth

Ernesto 12/5/2015 09:40
Deleted: that can be used to
Ernesto 12/5/2015 09:41
Deleted: in the determination of the
Ernesto 12/5/2015 09:43
Deleted: ,

51

1 Introduction

52 The assessment of uncertainties of snow measurements remains a challenging problem in
53 snow science. Snow cover properties are highly heterogeneous over space and time and the
54 representativeness of measurements of snow stage variables (e.g., snow depth, snow density, and
55 snow water equivalent (SWE)) is often overlooked due to difficulties associated with the
56 assessment of such uncertainties. This has been, at least in part, due to the limited knowledge of
57 the characteristics of the spatial statistical properties of variables such as snow depth and SWE,
58 particularly at the small-scales (sub-meter to tens of meters). However, recent improvements in
59 remote sensing of snow (e.g., light detection and ranging (LiDAR) and Radar technologies) have
60 allowed significant progress in the quantitative understanding of the small-scale heterogeneity of
61 snow covers in different environments (e.g., Trujillo et al., 2007; Trujillo et al., 2009; Mott et al.,
62 2011).

63 Point or local measurements of snow properties will continue to be necessary for purposes
64 ranging from inexpensive evaluation of the amount of snow over a particular area, to validation
65 of models and remote sensing measurements. Such measurements have a footprint representative
66 of a very small area surrounding the measurement location (i.e., support, following the
67 nomenclature proposed by Blöschl (1999)), and the integration of several measurements is
68 necessary for a better representation of the snow variable in question over a given area. Because
69 of this, tools for quantitative evaluations of the representativeness and uncertainty of
70 measurements need to be introduced, and the uncertainty of such measurements should be more
71 widely discussed in the field of snow sciences.

72 Currently, efforts to assess the reliability and uncertainty of snow measurements have
73 focused on statistical analyses using point measurements (e.g., Pomeroy and Gray, 1995; Yang

Ernesto 12/5/2015 09:45

Deleted: s

Ernesto 12/5/2015 09:45

Deleted: a turning point has been reached in recent years thanks to

Ernesto 12/5/2015 09:46

Deleted: , which

Ernesto 12/5/2015 09:46

Deleted: , with resolutions and areas of coverage previously unresolved with the standard methods of measurement

Ernesto 12/5/2015 09:47

Deleted: that

Ernesto 12/5/2015 09:47

Deleted: e

83 and Woo, 1999; Watson et al., 2006; Rice and Bales, 2010; Lopez-Moreno et al., 2011; Meromy
84 et al., 2013) or synthetically generated fields in a Monte Carlo framework (e.g., Kronholm and
85 Birkeland, 2007; Shea and Jamieson, 2010), comparisons between remotely sensed and ground
86 data (e.g., Chang et al., 2005; Grünewald and Lehning, 2014), and analyses of subsets drawn
87 from spatially distributed remotely sensed data (e.g., McCreight et al., 2014). These studies have
88 been useful to empirically quantify uncertainties associated with point measurements. For
89 example, Pomeroy and Gray (1995) present an equation for determining the minimum number of
90 surveys points required to be confident that the mean falls within a certain envelop around the
91 sample mean based on the CV of SWE or snow depth. McCreight el al. (2014) use the NASA's
92 Cold Land Processes Experiment (CLPX) LIDAR snow depth dataset (also used in this study) to
93 empirically address questions regarding the inference of larger-scale snow depths from sparse
94 observations. They evaluate estimation uncertainty from random sampling for varying sample
95 size. Their conclusions indicate that adding observations to a randomly distributed survey pattern
96 leads to a reduction in both percent-error in snow volume over the study areas, as well as its
97 uncertainty. They also add that with a few hundred observations, one can expect to infer the true
98 mean snow depth over the 1-km² domains to within 2% error. Despite of these insights, these
99 type of empirical approaches can be site-dependent, they do not provide a theoretical quantitative
100 framework for the assessment of uncertainties associated with a particular sampling design, they
101 do not allow for an optimal sampling strategy (e.g., selecting the number of points and locations
102 for a desired accuracy level), and they do not take advantage of the increased knowledge of the
103 characteristics of the heterogeneity of snow cover properties.

Ernesto Trujillo 18/5/2015 15:05

Deleted: and

Ernesto Trujillo 18/5/2015 18:17

Deleted: However

104 Another possible approach is one in which the expected error in the estimation of a particular
105 statistical moment of a field over a defined domain (e.g., areal mean or standard deviation from a

109 finite number of measurements) is determined on the basis of known statistical properties of the
110 field in question. Such approach uses geostatistical principles that have been proposed by
111 Matheron (1955; 1970) and others, and that have been applied in mining geostatistics (Journel
112 and Huijbregts, 1978), the analysis of uncertainties in measuring precipitation (Rodríguez-Iturbe
113 and Mejía, 1974), and for a more general analysis of the effects of sampling of random fields as
114 examples of environmental variables (e.g., Skøien and Blöschl, 2006), Implementation of these
115 types of approaches appear to be lacking in the numerous studies using point measurements to
116 represent snow distribution. Often in these studies, the spatial snow distribution derived from
117 point measurements is addressed as the “true” distribution, which is then used for evaluating the
118 performance of interpolation methodologies, regressions trees, and hydrological models. These
119 comparisons ignore the intrinsic error incurred when extrapolating the original point
120 measurements, leaving a proportion of uncertainty unaccounted for that can be significant. The
121 principal motivation of the present study is to encourage the use of more objective and
122 quantitative methodologies for error evaluation in snow sciences. The approach presented below
123 can be used for objective survey design to estimate snow distribution from point measurements.
124 We do not intend to present our approach as novel in the general geostatistical sense; instead, we
125 present the derivation with the specific application for snow sciences in mind. However, because
126 of the general nature of the random fields’ theory the development is based on, similar
127 developments can indeed be applied to other environmental variables that can be described as a
128 random field.

129 On this basis, the error in the estimation of spatial means from point measurements over a
130 particular domain (e.g., a profile, or an area) can be quantified as the expected value of the
131 squared difference between the real mean and the sample mean obtained from a limited number

Ernesto 12/5/2015 09:53

Deleted: when

Ernesto 12/5/2015 09:49

Deleted: , among others

Ernesto 12/5/2015 09:53

Deleted: Despite of these examples, there is to the authors’ knowledge no attempt of implementing such type of approach in snow sciences, tailoring the methodology to the particular analysis of uncertainties when measuring snow variables such as snow depth. Such an i

Ernesto 12/5/2015 09:53

Deleted: s

Ernesto 12/5/2015 10:01

Deleted: that

Ernesto 12/5/2015 10:01

Deleted: e

Ernesto 12/5/2015 10:08

Deleted: ,

Ernesto 12/5/2015 10:03

Deleted: addressing

Ernesto 12/5/2015 10:08

Deleted: the spatial

Ernesto 12/5/2015 10:14

Deleted: extrapolation of such point measurements as the “true” spatial distribution of snow depth when

Ernesto 12/5/2015 10:15

Deleted: unaccounted for

Ernesto 12/5/2015 10:15

Deleted: This

Ernesto 12/5/2015 10:15

Deleted: is

Ernesto 12/5/2015 10:17

Deleted: , with the intention of spreading

Ernesto 12/5/2015 10:17

Deleted: Also, t

Ernesto 12/5/2015 10:17

Deleted: that is

Ernesto 12/5/2015 10:19

Deleted: that

155 of point measurements. Such an approach, as it will be shown here, uses spatial statistical
156 properties of snow depth fields in a way that allows for an objective evaluation of the estimation
157 error for snow depth measurements. The sections below illustrate the use of such methodology
158 for optimal design of sample strategies in the specific context of snow depth. However, the
159 methodology can also be implemented for other snow variables such as snow water equivalent.

Ernesto 12/5/2015 10:10

Deleted: , given that similar geostatistics can be used to characterize their spatial organization

160

2 Background

161 Let $Z(\mathbf{x})$ denote a random field function of the coordinates \mathbf{x} in the n -dimensional space
162 \mathbb{R}^n . Bold letters represent a location vector from hereon. In our case, the field can represent e.g.:
163 snow depth or snow water equivalent (SWE) at a given time of the year. The mean of the process
164 over a domain A (e.g., a profile section or an area) is defined as:

165

$$\mu_z(A) = \frac{1}{A} \int_A z(\mathbf{x}) d\mathbf{x} \quad (1)$$

Unknown

Field Code Changed

166 In practice, the mean is often obtained from the arithmetic average of measurements at a
167 finite number of locations, N , within the domain:

168

$$\bar{Z} = \frac{1}{N} \sum_{i=1}^N z(\mathbf{x}_i) \quad (2)$$

Unknown

Field Code Changed

169 The performance of the estimator \bar{Z} can be evaluated by calculating the expected value of
170 the square difference between the estimator \bar{Z} and the true mean $\mu_z(A)$

171

$$\sigma_{\bar{Z}}^2(A) = E \left[\left(\frac{1}{N} \sum_{i=1}^N z(\mathbf{x}_i) - \frac{1}{A} \int_A z(\mathbf{x}) d\mathbf{x} \right)^2 \right] \quad (3)$$

Unknown

Field Code Changed

174 For a 1st order stationary process (i.e., the mean independent of location; e.g., Cressie (1993),
 175 section 2; and Journel and Huijbregts (1978), section 2), (3) can be expressed as

$$\begin{aligned}
 \sigma_z^2(A) &= \frac{1}{N^2} \sum_{i=1}^N VAR[z(\mathbf{x}_i)] + \frac{2}{N^2} \sum_{i=1}^{N-1} \sum_{j=i+1}^N COV[z(\mathbf{x}_i)z(\mathbf{x}_j)] \\
 &- \frac{2}{N \cdot A} \sum_{i=1}^N \int_A COV[z(\mathbf{x}_i)z(\mathbf{x}_j)] d\mathbf{x}_j \\
 &+ \frac{1}{A^2} \int_A \int_A COV[z(\mathbf{x}_i)z(\mathbf{x}_j)] d\mathbf{x}_i d\mathbf{x}_j
 \end{aligned} \tag{4}$$

177 where VAR[] and COV[] are the variance and the covariance, respectively. If we further
 178 assume that the process is second order stationary (e.g., Cressie (1993), section 2; and Journel
 179 and Huijbregts (1978), section 2), that is, if the mean and the variance are independent of the
 180 location, and the covariance function depends only on the vector difference $\mathbf{x}_i - \mathbf{x}_j$, (3) can be
 181 expressed as

$$\sigma_z^2(A) = \sigma_p^2 \left[\begin{aligned} &\frac{1}{N} + \frac{2}{N^2} \sum_{i=1}^{N-1} \sum_{j=i+1}^N CORR[\mathbf{x}_i - \mathbf{x}_j] \\ &- \frac{2}{NA} \sum_{i=1}^N \int_A CORR[\mathbf{x}_i - \mathbf{x}_j] d\mathbf{x}_j \\ &+ \frac{1}{A^2} \int_A \int_A CORR[\mathbf{x}_i - \mathbf{x}_j] d\mathbf{x}_i d\mathbf{x}_j \end{aligned} \right] \tag{5}$$

183 where CORR[] is the correlation function, and σ_p^2 is the variance of the point process.

184 The first two terms in (5) are the total sum of the covariances (or correlation as σ_p^2 has been
 185 factored out) between all point locations $i = 1, \dots, N$ (e.g., measurement locations). The first of
 186 the two terms is only a function of the number of points, while the second is a function of the
 187 number of points, N , and the correlations between the locations. Such correlations are themselves

Unknown
 Field Code Changed

Unknown
 Field Code Changed

188 a function of the separation vectors (both in magnitude and direction), and the parameters of the
189 correlation function. These two terms are independent of the size of the area A , and can be
190 thought of as the portion of the error caused by the correlation between the point processes at the
191 locations $i = 1, \dots, N$ (e.g., measurement locations). Term 3 accounts for the correlation between
192 the measurement locations and the continuous process over the domain A . This term can be seen
193 as a negative contribution to the total error assuming that the sum of the integrals is positive. The
194 term is a function of the number of points, N , the domain area, A , the location of the points and
195 the correlation structure, characterized using the parameters of the correlation function. Lastly,
196 term 4 is the contribution to the error caused by the intrinsic correlation structure of the
197 continuous process over the domain. This term is a function of the domain (e.g., size and shape
198 of A) and the correlation structure (e.g., parameters of the correlation function).

199 **3 Data**

200 For the analyses and tests of the methodology presented here, Light Detection and Ranging
201 (LIDAR) snow depths obtained as part of the NASA's Cold Land Processes Experiment (CLPX)
202 will be used (Cline et al., 2009). The dataset consists of spatially distributed snow depths for 1-
203 km x 1-km areas (Intensive Study Areas - ISAs) in the Colorado Rocky Mountains close to
204 maximum snow accumulation in April, 2003. The data were processed from snow-on (8-9 April,
205 2013) and snow-off (18-19 September, 2013) LIDAR elevation returns with an average
206 horizontal spacing of 1.5 m and vertical tolerance of 0.05 m. The final CLPX snow depth
207 contour product (0.10 m vertical spacing) was generated from these returns. This product was
208 used to generate gridded snow depth surfaces with 1024x1024 elements over the ISAs, for a grid
209 resolution of 0.977 m. For this study two areas will be used: the Fraser – St Louis Creek ISA
210 (FS) and the Rabbit Ears – Walton Creek ISA (RW) (Figure 1). The FS ISA is covered by a

211 moderate density coniferous (lodgepole pine) forest on a flat aspect with low relief. The RW ISA
212 is characterized by a broad meadow interspersed with small, dense stands of coniferous forest
213 and with low rolling topography. The snow depth distributions in these ISAs show differences
214 that are relevant for the analysis of the methodology introduced here. At the FS ISA, the snow
215 depth distribution is relatively isotropic (Figure 1b), with short spatial correlation memory and
216 little variations in the spatial scaling properties (i.e., power-spectral exponents and scaling
217 breaks) with direction (Trujillo et al., 2007). On the other hand, the spatial distribution of snow
218 depth in the RW ISA is more anisotropic (Figure 1c), with longer spatial correlation memory
219 along a principal direction aligned with the predominant wind direction versus shorter memory
220 along the perpendicular direction, and with variations in the power-spectral exponents and
221 scaling breaks according to the predominant wind directions (Trujillo et al., 2007).

222 **4 One-dimensional process**

223 The spatial representation of the snow cover requires a basic assumption on the scale or
224 resolution at which a field or profile is going to be represented. This relies on the spatial support
225 of the measurements. For the case of snow depths, point measurements from local surveys using
226 a snow depth probe are frequently used for this representation. Generally, there are additional
227 sources of uncertainty associated with these types of measurements, such as the accuracy of the
228 position of the measurement in space or deviations in the vertical angle of penetration of the
229 probe through the snow pack. These uncertainties are additional to any of the uncertainties
230 estimated using the methodology discussed here.

231 The one-dimensional case provides a good opportunity to illustrate the limitations of point
232 measurements. Consider the case of a snow depth profile that is measured using a snow depth
233 probe at a regular spacing “d”. Each of these point measurements is meant to represent the mean

234 | snow depth over a particular distance surrounding the measurement. The question is: over what
235 | distance is [this](#) assumption valid? In this case, the intrinsic assumption is that the measurement is
236 | representative over the distance “d”, but at this point the validity of such [an](#) assumption is not
237 | proven.

Ernesto 12/5/2015 10:53

Deleted: ,

Ernesto 12/5/2015 10:53

Deleted: and t

Ernesto 12/5/2015 10:53

Deleted: such

238 | The answer to this question is conditioned to how variable the profile is and over what
239 | distances. To [address](#) this, let us look at two snow depth profiles, one in a forested environment
240 | (FS) and another in an open environment (RW) in the Colorado Rocky Mountains (Figure 2a and
241 | Figure 3a, respectively). The variability in the profiles is markedly different, with variations over
242 | shorter distances in the forested area, and a smoother profile in the open and wind influenced
243 | environment. This is reflected in the spatial correlation structure of these snow depth profiles,
244 | with stronger correlations over longer distances in open and wind-influenced environments with
245 | respect to that in forested environments (Trujillo et al., 2007; Trujillo et al., 2009). These
246 | differences should be considered when selecting the sampling frequency required to capture the
247 | variability and accurately represent the mean conditions within a particular sampling spacing.
248 | This is illustrated by comparing the mean snow depth for a particular resolution to the point
249 | value at the center of the interval (Figure 2b in a forested environment and Figure 3b in an open
250 | and wind-influenced environment). In the Figures, average versus point values at several
251 | sampling intervals are compared for normalized profiles ($\mu = 0$, $\sigma = 1$) separated every 30 m in
252 | both the x (east) and y (north) directions and for an area of 500 m by 500 m. The 30-m separation
253 | between profiles is chosen to reduce the spatial correlation between them.

Ernesto 12/5/2015 10:54

Deleted: look at

254 | Firstly, the resulting comparison shows that the point values generally overestimate the
255 | variability in mean snow depths if we replace the mean snow depth distribution by its point
256 | sample. To clarify this, let us consider here two snow depth profiles, one with the snow depths at

261 the nominal scale (~1 m), and a second one with a moving average (MA) of the first one with an
262 averaging window equal to the sampling spacing. Ultimately, the variance/standard deviation of
263 the first profile (~1 m) is larger than that of the MA, with a distribution that reflects these
264 differences. The samples drawn from the first profile will reflect a larger variance than that of the
265 samples from the MA profile as they are drawn from these distributions, and this is what is
266 reflected in Figure 2 and Figure 3. The degree of overestimation can be quantified through the
267 slope of the regression line (in red in Figure 2b and Figure 3b). In the forested environment
268 (Figure 2b), the slopes range between 0.8 and 0.13, with decreasing slopes with increasing
269 spacing. These slopes indicate that, on average, the mean values are 0.8 times the point values
270 for the 5 m spacing and 0.1 times the point values for the 100 m spacing. In the open and wind-
271 dominated environment, the slopes are higher and range between 0.97 and 0.23 from 5 m spacing
272 and 100 m spacing, respectively. A clear difference emerges: forested environments require
273 shorter separation between single measurements if the snow depth profile is to be accurately
274 captured by the measurements. The variability within the size of the interval determines the
275 degree of uncertainty associated with the point measurements, as the sub-interval variability is
276 related to the degree of overestimation of the mean value within the interval.

277 Secondly, the differences between average and point values for each spacing distance are
278 generally more scattered in the forested environment than in the open environment, and in both
279 environments the degree of scattering increases with spacing (Figure 2c and Figure 3c).
280 However, it is important to note here that we are comparing normalized profiles ($\mu = 0, \sigma = 1$),
281 allowing us to focus on the rescaled spatial variations. What is highlighted is the relevance of the
282 spatial structure of the profile rather than the absolute variance. This spatial structure can be
283 quantified by, for example, the spatial covariance/correlation function.

284 | In addition to differences in correlation structure, there are also differences in the absolute
285 | variability in snow depth in these environments (Figure 4). Contrary to the normalized snow
286 | depth discussed above, the subinterval standard deviation as a function of interval size along the
287 | profiles is higher in the open and wind-influenced environment at RW versus the forested
288 | environment at FS (Figure 4a). Mean standard deviation values in the open environment are
289 | twice as large as those at the forested environment towards the larger interval sizes (~100 m).
290 | The standard deviation increases with interval size in both environments, with the steepest
291 | increase at the lower interval sizes. Furthermore, the standard deviation tends to stabilize more
292 | rapidly in the forested environments, with an increase of only 1.8 cm between 30 m and 100 m.
293 | On the other hand, the standard deviation continues to increase in the open environment at RW,
294 | with less of an asymptotical behavior for the scales analyzed. Complementary, the shaded areas
295 | (25% to 75% quantiles) give an idea of the variability of standard deviation values, with a much
296 | wider range in RW versus FS, and an increase in the range between quantiles with interval size
297 | in RW.

298 | Consistent with the standard deviation, the sub-interval mean range (range defined as the
299 | difference between the maximum and minimum snow depths within an interval) increases with
300 | interval size in both FS and RW (Figure 4b). However, the mean range is larger in the open
301 | environment at RW and the rate of increase with interval size is also steeper. Similarly, the
302 | shaded areas indicate wider distribution of range values in the open environment at RW, while
303 | relatively uniformly distributed around the mean across interval sizes in the forested environment
304 | at FS. The results in Figure 2-Figure 4 illustrate this contrasting behavior between the snow
305 | covers in these environments and their influence on measurement strategies: that is, the forested
306 | environments requires shorter separation between measurements for accurate representation of

Ernesto 12/5/2015 10:55

Deleted: Additionally

Ernesto 12/5/2015 10:55

Deleted: the

Ernesto 12/5/2015 10:55

Deleted: the

Ernesto 12/5/2015 10:55

Deleted: As opposed

311 the snow cover, however, in the wind-influence and open environment, the subinterval
312 variability is higher indicating wider variations around any sampled measurement within the
313 interval.

314 Ultimately, the number and distance between measurements and the specific arrangement of
315 the measurements are all conditioned to what the measurements are needed for. Hydrologic
316 applications may not require a highly detail representation of a snow depth profile (or a field),
317 and representing the average conditions over a given distance (or area) is sufficient, but small-
318 scale process-based studies may require a more detailed characterization over shorter distances
319 (or smaller areas). This implies that the decision depends on the particular use that the
320 measurements will support. In the following sections, the equations presented in the Background
321 (section 2) will be applied to evaluate the uncertainty associated with multiple measurement
322 designs for profiles and fields of snow depth.

323 4.1 Case 1: Single measurement along a profile section

324 Equation (2) can be used to evaluate the uncertainty of a single measurement along a profile
325 section of length L . For this case, as well as for the following cases in this article, an exponential
326 covariance with a decay exponent ν ($\nu > 0$) will be assumed:

$$327 \quad COV(\mathbf{h}, \sigma, \nu) = \sigma^2 \exp(-\nu \|\mathbf{h}\|) \quad \text{for } \sigma^2 > 0, \text{ and } \nu > 0 \quad (6)$$

328 where σ^2 is the variance, and $\|\mathbf{h}\|$ is the length of the vector \mathbf{h} . For this one-dimensional case
329 and combining (6) and (5), the following expression is obtained:

$$330 \quad \sigma_z^2(x, L, \nu) / \sigma_p^2 = 1 - \frac{2}{Lv} \left[2 - \exp(-\nu x) - \exp(-\nu \cdot [L - x]) \right] + \frac{1}{L^2 \nu} \left[2L + \frac{2}{\nu} \exp(-\nu L) - \frac{2}{\nu} \right]$$

331 (7)

Unknown
Field Code Changed

Unknown
Field Code Changed

332 where x is the distance from one extreme of the section to the location of the measurement
333 (Figure 5a). The normalized squared error $\sigma_z^2(x, L, v) / \sigma_p^2$ is minimized at x equal to half of the
334 section length, $L/2$, regardless of v . The existence of a correlation in the profile leads to this
335 solution, as the middle location contains more information about its surroundings. Also, this
336 solution is different from the solution for an uncorrelated profile (e.g., white noise), for which
337 the squared error would be equal to the variance, independent of the location of the
338 measurement.

339 The results here are confirmed with an analysis of LIDAR snow depths profiles in FS and
340 RW (Figure 6). The analysis consists of calculating the difference between the mean and the
341 point value for sections of a given length (varied between 10 m – 50 m) and for x (Figure 5a)
342 between 0 and L along the profile sections. Each sample section of length L will provide a single
343 difference for each of the x values. These sample differences are then used to calculate the mean
344 normalized squared error for each x , and the same is repeated for each section length L . The
345 results indicate that the real snow depth profiles behave as predicted by the model of the error,
346 with a minimum error at x equal to half of the section length. Another difference highlighted by
347 these results is the difference between the sample errors in the forested environment (FS) versus
348 the open environment (RW) for the larger interval sizes (e.g., 50 m). The sampled normalized
349 squared error in the forested environment shows only a mild decrease in the square error to
350 around 0.7-0.8 towards the inside of the section length. However, this decrease is achieved for
351 the measurement along most of the interval length with the exception of the extremes. This can
352 be explained by the relationship between the spatial memory of snow depth (e.g., the correlation
353 function) and the section length. Densely forested environments exhibit correlation lengths that
354 are shorter than those in open and wind influenced environments (e.g., Trujillo et al., 2007;

Ernesto Trujillo 19/5/2015 11:38

Deleted: Figure 6

356 Trujillo et al., 2009). As the section length increases beyond such correlation lengths, a
357 measurement location towards the middle of the interval contains less information of the
358 surrounding snow depths in a forested environment (e.g., FS) versus an open and wind
359 influenced environment (e.g., RW). This is observed in [Figure 6c](#) versus [Figure 6f](#), with the
360 results in RW showing a more clear minimum towards the center of the profile section. The
361 results also show a poorer performance of the model in RW versus FS, as the exponential
362 correlation model has a poorer fit in RW at the shorter-lag range; However, model performance
363 is improved for longer section lengths (e.g., [Figure 6c](#) and [f](#))

364 Model and sampled results thus support that the measurement location can be fixed in the
365 middle of the interval, and the normalized squared error can then be described as a function of
366 both the exponential decay exponent, ν , and the length of the section, L ([Figure 7a](#)). The
367 normalized squared error increases with interval length, with a steeper increase for larger
368 exponential decay exponents, for which the squared error approaches that of an uncorrelated
369 field more rapidly. The theoretical model is tested on the snow depth fields at FS and RW. The
370 test consists of calculating the sampled normalized squared error as the average of all squared-
371 differences between the mid-section snow depth and the mean from all LIDAR grid-points
372 within each interval of length L . This is done for profiles separated every 30 m, similar to the
373 analysis above, and for profiles along the x and y directions. The theoretical normalized squared
374 error is estimated from (7) using the exponential decay exponent from the model fitted to the
375 sampled correlation function. The results show that the theoretical model reproduces the sampled
376 squared error remarkably well, even reproducing the anisotropic properties of the correlograms,
377 represented by the different exponents of the exponential model along x and y directions ([Figure](#)
378 [7b](#) and [c](#)). The model also reproduces the different behavior of the squared error between both

Ernesto Trujillo 19/5/2015 11:38

Deleted: Figure 6

Ernesto Trujillo 19/5/2015 11:38

Deleted: Figure 6

Ernesto Trujillo 19/5/2015 11:38

Deleted: Figure 6

Ernesto 12/5/2015 11:01

Deleted: ,

Ernesto Trujillo 19/5/2015 11:38

Deleted: Figure 7

Ernesto Trujillo 19/5/2015 11:38

Deleted: Figure 7

385 fields (i.e., FS and RW), showing that the normalized squared error increases more rapidly and is
 386 larger in the forested environment (Figure 7b) versus the open environment (Figure 7c).
 387 However, it should be noted here that as the error is normalized and as the variance of the field in
 388 the open environment is larger (Figure 4a), the absolute squared error could reach higher values
 389 in the open environment (RW). In this regard, one feature to discuss here is the assumption that
 390 the point variance of snow depth in these environments has been estimated as the spatial variance
 391 over the entire study area, as it is generally practiced in time series analysis and geostatistics. In
 392 practice, this is the only possible approach because there is limited information to estimate the
 393 point variance from multiple realizations of the process at each spatial location, as inter- and
 394 intra- annual snow depth fields are not available, not only for these areas, but for almost any area
 395 where this methodology may be applied.

396 4.2 Case 2: Three measurements along a profile section

397 From (5) it is also evident that increasing the number of measurements will reduce the
 398 squared error. In the case of three measurements separated by a distance 'a', with the middle
 399 measurement centered in the section of length L (Figure 5b), and for an exponential covariance
 400 function with parameter v, (5) leads to the following expression for this particular case:

$$\begin{aligned}
 \sigma_{\frac{z}{2}}^2(a, L, v) / \sigma_p^2 &= \frac{1}{3} + \frac{2}{9} [2 \exp(-va) - \exp(-2va)] \\
 &- \frac{4}{3Lv} \left[3 - \exp\left(-\frac{vL}{2}\right) (1 + \exp(-va) + \exp(va)) \right] \\
 &+ \frac{1}{L^2 v} \left[2L + \frac{2}{v} \exp(-vL) - \frac{2}{v} \right]
 \end{aligned} \tag{8}$$

402 Equation (8) can be minimized to determine the optimal separation distance between points,
 403 a, as a function of L and v:

Ernesto Trujillo 19/5/2015 11:38

Deleted: Figure 7

Ernesto Trujillo 19/5/2015 11:38

Deleted: Figure 7

Unknown

Field Code Changed

Ernesto Trujillo 19/5/2015 11:39

Formatted: Default Paragraph Font

Ernesto Trujillo 19/5/2015 11:38

Deleted: (8)

407
408
409
410
411
412
413
414
415
416
417
418
419
420
421
422
423
424
425

$$a_{optimal} = -\frac{1}{v} \ln(t) \quad (9)$$

where

$$t = \frac{B + \sqrt{B^2 - 4AB}}{2A}$$

$$A = \frac{4v}{9}$$

$$\text{and } B = -\frac{4}{3L} \exp\left(-\frac{vL}{2}\right)$$

The combination of (8) and (9) can be used to determine the normalized squared error, σ_z^2 / σ_p^2 , and the optimal distance, $a_{optimal}$, for the measurement pattern in Figure 5b. The model predicts that the normalized squared error is minimized at an intermediate location between 0 and $L/2$ (black lines in Figure 8a and b). The results show an increase in the error with interval size, L , as well as little sensitivity of $a_{optimal}$ to v . This latter feature can be seen as an advantage since small biases in the estimation of v will not result in significant biases in the estimation of $a_{optimal}$. One could almost assume a value of $a_{optimal}$ without prior knowledge of the exponential decay exponent, selecting $a_{optimal}$ within the range of values indicated by the model for a range of possible exponential decay exponents. Note that $a_{optimal}$ is located close to the 60% distance from the center towards the outer boundary of the profile section for all section lengths (Figure 8a and b). On the other hand, the measurement error displays a higher sensitivity to v around $a_{optimal}$, indicating that biases in the estimation of v would have a more noticeable effect on the estimation of the measurement error. This is further clarified in Figure 8c, in which the normalized error (not squared) and $a_{optimal}$ can be obtained for corresponding profile section

Unknown
Field Code Changed

Ernesto Trujillo 19/5/2015 11:39
Formatted: Default Paragraph Font

Ernesto Trujillo 19/5/2015 11:38
Deleted: (8)

427 lengths (L) and exponential decay exponents (ν) based on the isolines shown. For example, for a
428 profile section of 30 m, and an exponential decay exponent of 0.2 m^{-1} , the normalized error is
429 0.32 and a_{optimal} is 9.63 m (see intersect of the two isolines in Figure 8c). The normalized error in
430 Figure 8c is not squared, highlighting the sensitivity of the measurement error to ν , which
431 represents the degree of spatial correlation of the profile in this case (e.g., lower values indicate
432 stronger spatial memory/correlation, hence lower measurement errors).

433 The performance of the model is tested against the normalized squared error obtained from
434 the same snow depth profiles in FS and RW. The test consists of estimating the normalized
435 squared error for profiles sections of length between 10 m and 80 m, with a being varied between
436 0 and $L/2$ (Figure 9). For each value of a , the normalized squared error is estimated based on the
437 means obtained using the three snow depth samples for each section. All squared differences are
438 then averaged to obtain the values presented in the Figure. Sampled and modeled errors follow
439 the same trend across all a values and for the different L values in Figure 9. The minimum error
440 is also reproduced by the model proving the applicability of the model for estimating the optimal
441 separation between measurements. The model does perform better in the forested environment of
442 FS versus RW, particularly for lower a values. This can be justified as the exponential
443 covariance model displays a better fit in FS over RW, particularly over the lower range of lag
444 values. Also, note that both the modeled and sampled normalized squared errors are lower for the
445 snow depth profiles at RW because of the longer spatial memory of the snow depth distribution
446 in this environment (higher spatial correlations) when compared to that in FS.

447 **4.3 Case 3: N measurements along a profile section**

448 As stated above, the measurement error can be reduced by increasing the number of
449 measurements taken over a given section of length L . Let us focus on the case of stratified

450 sampling where N regularly spaced measurements are taken over the interval (Figure 5c), and to
 451 quantify this reduction we can use (5) and the exponential covariance model. Equation (5) can
 452 then be reduced to:

$$\begin{aligned}
 \sigma_z^2(N, L, \nu) / \sigma_p^2 &= \frac{1}{N} + \frac{2}{N^2} \sum_{k=1}^{N-1} k \exp\left(-\nu \left[L - \frac{kL}{N} \right]\right) \\
 &- \frac{4}{Lv} \left[1 - \frac{1}{N} \sum_{k=1}^N \exp\left(-\nu \frac{L}{N} \left[N - k + \frac{1}{2} \right]\right) \right] \\
 &- \frac{2}{L^2 \nu^2} [1 - Lv - \exp(-\nu L)]
 \end{aligned} \quad (10)$$

454 The normalized squared error (σ_z^2 / σ_p^2) obtained with (10) for profiles sections of lengths
 455 between 10 and 80 shows a steep decrease with N (Figure 10), with a steeper decrease for higher
 456 exponential decay exponents. For the longer profile sections (e.g., 80, Figure 10d), small
 457 reductions in the squared error are achieved beyond only a few measurements (e.g., $N = 16$).
 458 Equation (10) and the results in Figure 10 can be used to determine the number of measurements
 459 necessary to achieve a desired accuracy level. One could, for example, design a survey to sample
 460 a snow depth profile with a mean value every 10 m. The number of measurements required to
 461 achieve a desired level of accuracy can be obtained from Figure 10a, based on previous
 462 knowledge of the sample estimate of the exponential decay exponent. This can be achieved
 463 thanks to the intra-annual and inter-annual persistence of the spatial patterns, and hence, the
 464 spatial statistical properties of snow depth fields in mountain environments, as shown in previous
 465 studies using both manual surveys and LIDAR measurements (e.g., Deems et al., 2008; Sturm
 466 and Wagner, 2010; Schirmer et al., 2011; Melvold and Skaugen, 2013; Helfrich et al., 2014). A
 467 detailed spatial survey (e.g., dense manual measurements or TLS), sampling different portions of
 468 an area can be used to determine the covariance/correlation characteristics of the snow depth

Unknown
 Field Code Changed

Ernesto Trujillo 19/5/2015 11:39
 Formatted: Default Paragraph Font
 Ernesto Trujillo 19/5/2015 11:38
 Deleted: (10)

Ernesto 12/5/2015 11:03
 Deleted: little
 Ernesto 12/5/2015 11:03
 Deleted: are achieved

Ernesto Trujillo 19/5/2015 11:39
 Formatted: Default Paragraph Font
 Ernesto Trujillo 19/5/2015 11:38
 Deleted: (10)

473 distribution, with which the model for the error can be applied. An a priori estimate of the
474 exponential decay exponent may also be possible and will be tested in future applications of the
475 framework, given the relative insensitivity of the error with respect to ν .

476 Following the method described in the previous section, we test the performance of the
477 model against the normalized squared error obtained from the same snow depth profiles in FS
478 and RW. In this case, the sampled squared error is estimated based on the N regularly-spaced
479 measurements distributed along the profile sections of length L . As the snow depth fields are
480 gridded at ~ 1 -m resolution, the location of the measurements is approximated to the closest
481 coordinate in the profile section following the pattern in Figure 5c. Once again, sampled and
482 modeled errors follow closely the same trend for the different L values in both FS and RW
483 (Figure 11). The error decreases with N , with a rapid decay at the lower N values, illustrating that
484 the error can be drastically reduced by simply increasing the number of measurements by a small
485 amount. The normalized squared error across all N values is lower for RW than for FS,
486 consistent with the higher spatial correlations observed in the snow depth fields of RW versus
487 FS. Once again, there are some differences between the sampled and modeled normalized
488 squared error in RW for the shorter profile lengths and for small N values: a consequence of the
489 poorer fit of the exponential model for the shorter lag range in RW. However, the model is still
490 able to reproduce the error in both fields, and the applicability of the model is illustrated even
491 when the fit of the correlation model can be improved.

492 **5 Two-dimensional process**

493 Similar to the one-dimensional process, equation (5) can be formulated to calculate the
494 squared error in the two-dimensional space. To exemplify this, we apply the methodology to an
495 isotropic process over the x - y plane for three cases in a square area: (a) one single measurement

496 in the center of the area, (b) five measurements radiating out from the center (Figure 12a), and
 497 (c) N by N measurements regularly spaced in the x and y directions (Figure 12b).

498 For the isotropic case, the covariance/correlation function is only dependent on the
 499 magnitude of the lag vector,

500
$$h_{i,j} = |\mathbf{x}_i - \mathbf{x}_j| \quad (11)$$

Unknown
Field Code Changed

501

502 and, consequently, the error is represented by,

503
$$\sigma_z^2(A) = \sigma_p^2 \left[\begin{aligned} & \frac{1}{N} + \frac{2}{N^2} \sum_{i=1}^{N-1} \sum_{j=i+1}^N CORR[h_{i,j}] \\ & - \frac{2}{NA} \sum_{i=1}^N \int_A CORR[h_{i,j}] d\mathbf{x}_j \\ & + \frac{1}{A^2} \int_A \int_A CORR[h_{i,j}] d\mathbf{x}_i d\mathbf{x}_j \end{aligned} \right] \quad (12)$$

Unknown
Field Code Changed

504

505 The exponential correlation function for the isotropic case takes the following form:

506
$$CORR(h,v) = \exp(-vh) \quad (13)$$

Unknown
Field Code Changed

507 where h is the magnitude of the lag vector. Replacing into the expression for σ_z^2 , we obtain,

508
$$\sigma_z^2 = \sigma_p^2 \left[\begin{aligned} & \frac{1}{N} + \frac{2}{N^2} \sum_{i=1}^{N-1} \sum_{j=i+1}^N \exp(-v|\mathbf{x}_i - \mathbf{x}_j|) \\ & - \frac{2}{NA} \sum_{i=1}^N \int_A \exp(-v|\mathbf{x}_i - \mathbf{x}_j|) d\mathbf{x}_j \\ & + \frac{1}{A^2} \int_A \int_A \exp(-v|\mathbf{x}_i - \mathbf{x}_j|) d\mathbf{x}_j d\mathbf{x}_i \end{aligned} \right] \quad (14)$$

Unknown
Field Code Changed

509 For the case of a rectangular area of side dimension L_x and L_y in the corresponding x and y
 510 directions, the equation becomes,

$$511 \quad \sigma_z^2 = \sigma_p^2 \left[\begin{aligned} & \frac{1}{N} + \frac{2}{N^2} \sum_{i=1}^{N-1} \sum_{j=i+1}^N \exp\left(-v\left((x_i - x_j)^2 + (y_i - y_j)^2\right)^{1/2}\right) \\ & - \frac{2}{NA} \sum_{i=1}^N \int_0^{L_y} \int_0^{L_x} \exp\left(-v\left((x_i - x)^2 + (y_i - y)^2\right)^{1/2}\right) dx dy \\ & + \frac{1}{A^2} \int_0^{L_y} \int_0^{L_x} \int_0^{L_y} \int_0^{L_x} \exp\left(-v\left((x' - x)^2 + (y' - y)^2\right)^{1/2}\right) dx dy dx' dy' \end{aligned} \right] \quad (15)$$

512 The limits of the integrals can be changed depending on the desired location of the origin. In
 513 this case, the origin is located at the lower-left corner.

514 As discussed earlier, the first term is only a function of N , such that the base error is the
 515 variance of the point process divided by the number of points. The second term is a function of
 516 N , the location of the points, and the decay rate v . The third term is a function of N , A , the
 517 location of the points, and the decay rate v . The fourth term is a function of A and v , but is
 518 independent of the location of the points and N (i.e., independent of the survey design, and only a
 519 function of the correlation structure of the continuous process).

520 5.1 Case 1: Single measurement in the center of the area

521 In this case, we focus on a single measurement in the middle of a square area of side
 522 dimension L . Numerical solution of (15) shows that the normalized squared error increases
 523 rapidly with L , with a steeper increase for higher exponential decay exponents (Figure 13a),
 524 which approach a normalized squared error of 1 for L values less than 10 (e.g., $1 \leq v \leq 5$). The
 525 theoretical results in Figure 13a can be used to determine the discrepancy between a single
 526 measurement in the middle of an area and the areal mean for a second order stationary and
 527 anisotropic process with an exponential covariance/correlation function. Comparison of the

Unknown
 Field Code Changed

Ernesto Trujillo 19/5/2015 11:39
 Formatted: Default Paragraph Font
 Ernesto Trujillo 19/5/2015 11:38
 Deleted: (15)

529 modeled and sampled normalized square errors for the FS snow depth field indicate very good
530 agreement between modeled and sample errors (Figure 13b). The sample error is estimated
531 following the same procedure explained for the one-dimensional cases, although in the two-
532 dimensional space. Both sampled and modeled errors show the same behavior across L values
533 between 1 m and 100 m, although the scatter in the sampled error increases for larger L values.
534 This can be explained by the smaller number of samples to estimate the mean normalized
535 squared error and the fact that the correlation structure decays rapidly and a single sample
536 becomes less correlated to the surrounding area for these larger areas. The model introduced here
537 can then be used to assess the representativeness of a single measurement over an area
538 objectively and accurately, and it can be extended for other covariance/correlation functions as
539 needed.

540 5.2 Case 2: Five measurements radiating out from the center of the area

541 | The case of five measurements radiating out from the center (Figure 12a), with a point in the
542 | middle of the area and four points separated by a distance a from the center leads to a similar
543 | optimization problem as illustrated in case 2 of the one-dimensional examples (section 4.2). In
544 | the two-dimensional case, (15) does not have an explicit solution for a , and numerical
545 | implementation is required. The equation can be solved by simply replacing the point
546 | coordinates and the correlation function parameters. Following this approach, the normalized
547 | squared error can be obtained for areas of varying sizes (Figure 14). Similar to the one-
548 | dimensional example (case 2, section 4.2), σ_z^2/σ_p^2 decreases with a , reaching a minimum at an
549 | intermediate distance from the middle point outwards. The decay in σ_z^2/σ_p^2 is more rapid for
550 | the least correlated processes (i.e., higher decay exponents) reaching a value close to the base

Ernesto Trujillo 19/5/2015 11:39

Formatted: Default Paragraph Font

Ernesto Trujillo 19/5/2015 11:38

Deleted: (15)

552 normalized square error that is a function of the number of points (i.e., $1/N = 1/5$ in this case). An
553 extended analysis of the effect of each of the terms in the equation is included in the
554 Supplementary Information. The error, as shown in Figure 14, is minimized as a consequence of
555 two balancing terms that lead to this intermediate solution. The optimal solution is a balance
556 between reducing the correlation between the individual measurements (e.g., increasing the
557 separation between the location of the measurements) but increasing the correlation between the
558 measurements and the surrounding area (e.g., locating the measurements closer to the middle of
559 the area). These two competing effects lead to an optimization problem based on the location of
560 the point measurements. For the least correlated processes, the error resembles the behavior of an
561 uncorrelated field once the measurements become effectively decorrelated (e.g., $a > 1$ in Figure
562 14b for $\nu = 5$). Figure 14 exemplifies how (15) can be used to determine the optimal
563 measurement location for areas of different sizes, and to determine the associated error with
564 configurations other than the optimal.

565 The performance of the model is tested against the normalized squared error obtained from
566 the snow depth field in FS. The test consists of estimating the normalized squared error for a
567 square area with side length (L) between 10 m and 79 m, with a being varied between 0 and $L/2$
568 (Figure 15). For each value of a , the normalized squared error is estimated based on the means
569 obtained using the five snow depth samples for each section. All squared differences are then
570 averaged to obtain the values presented in the figure. Once again, the sampled and modeled
571 errors follow the same trend across all a values and for the different L values. The minimum
572 error and $a_{optimal}$ are also reproduced closely by the model, and as the area size increases, the
573 sampled and modeled error approach the error for an uncorrelated field at larger separations (i.e.,

Ernesto 12/5/2015 11:04

Deleted: behaves closer to

Ernesto Trujillo 19/5/2015 11:39

Formatted: Default Paragraph Font

Ernesto Trujillo 19/5/2015 11:38

Deleted: (15)

Ernesto 12/5/2015 11:05

Deleted: s of

Ernesto 12/5/2015 11:05

Deleted: dimension

578 0.2). These results illustrate that the performance of the model in the two-dimensional space is
579 remarkable, similar to what was observed in the one-dimensional case.

580 5.3 Case 3: N by N measurements regularly spaced in the x and y directions

581 Similar to the one-dimensional case, the two-dimensional case of N by N regularly spaced
582 measurements (Figure 12b) leads to a decreasing normalized squared error with N (Figure 16).

583 There is a sharp decrease in the error by just increasing the number of measurements in the lower
584 range of N . The analysis illustrates that stratified sampling, as shown here, is an excellent
585 approach for minimizing the error. For a 10 by 10 area for example, increasing N to 4 ($N^2 = 16$)
586 reduces the normalized squared error to less than 0.05. It is also worth noting here that for this
587 two-dimensional case, the error is less sensitive to the value of the exponential decay exponent
588 (ν) for the higher N values as the mean is accurately captured regardless of the correlation of the
589 field. Beyond a certain number of measurements regularly distributed in the area, the
590 measurements gather enough information such that there are only very minor improvements with
591 the addition of new measurements, regardless of the exponent value. Figure 16 serves as an
592 example of how the methodology can be used for objective selection of the number of
593 measurements necessary to achieve a desired accuracy level using prior knowledge of the spatial
594 covariance function.

595 The performance of the model is tested again for a square area with side length (L) between
596 10 m and 79 m using the snow depth field in FS, and for an increasing number of rows/columns
597 of measurements leading to a total number of measurements of N^2 (Figure 17). The results
598 illustrate again the accurate performance of the theoretical model, with sampled and model errors
599 following closely the same squared errors. Both sampled and modeled errors increase as the size

Ernesto 12/5/2015 11:10

Deleted: y

Ernesto 12/5/2015 11:11

Deleted: with

Ernesto 12/5/2015 11:11

Deleted: the one

Ernesto 12/5/2015 11:11

Deleted: to

Ernesto 12/5/2015 11:16

Deleted: For example, f

Ernesto 12/5/2015 11:15

Deleted: the

Ernesto 12/5/2015 11:17

Deleted: area of

Ernesto 12/5/2015 11:12

Deleted: s

Ernesto 12/5/2015 11:12

Deleted: of

Ernesto 12/5/2015 11:13

Deleted: dimension

610 of the area increases, as expected. These results complete the model performance tests for the
611 two-dimensional isotropic case.

612 **6 Summary and Conclusions**

613 A methodology for an objective evaluation of the error in capturing mean snow depths from
614 point measurements is presented based on the expected value of the squared difference between
615 the real average snow depth and the mean of a finite number of snow depth samples within a
616 defined domain (e.g., a profile section or an area). The model can be used for assisting the design
617 of survey strategies such that the error is minimized in the case of a limited and predetermined
618 number of measurements, or such that the desired number of measurements is determined based
619 on a predefined acceptable uncertainty level. The model is applied to one- and two-dimensional
620 survey examples using LIDAR snow depths collected in the Colorado Rockies. The results
621 confirm that the model is capable of reproducing the estimation error of the mean from a finite
622 number of samples for real snow depth fields.

623 Here, we should highlight some of the implications of the assumptions made in the model. In
624 simplified terms, the second-order stationarity assumption implies that the mean and the variance
625 of the process/variable (e.g., snow depth) are independent of the spatial location, and that the
626 covariance is dependent only on the separation vector (i.e., lag). Although these assumptions
627 may be less valid over larger scales (e.g., greater than 100 m), in the context of the model
628 application to snow depth the assumption should be valid at smaller scales, We present these
629 examples to show how the error can be quantified with good accuracy at such smaller scales.
630 Application of these types of approaches at larger scales will require additional evaluation, with
631 particular attention as to what the specific demands of the application are. Also, the methodology
632 presented here is not suitable for discontinuous snow cover, if both snow-covered and snow-free

Ernesto 12/5/2015 11:19

Deleted: not be as adequate

Ernesto 12/5/2015 11:21

Deleted: at smaller scales the assumption in the context of the model application to snow depth should be valid

Ernesto 12/5/2015 11:22

Deleted: round

Ernesto 12/5/2015 11:22

Deleted: such

Ernesto 12/5/2015 11:22

Deleted: s

Ernesto 12/5/2015 11:23

Deleted: as

Ernesto 12/5/2015 11:27

Deleted: s

642 areas are considered in the error estimation. This case has not been considered in the
643 development here.

644 Implementation of the model in practice requires prior assumption of a
645 correlation/covariance model and estimates of the model parameters (e.g., the decay exponent for
646 the exponential case). In the examples presented here we use LIDAR data for the parameter
647 estimation to illustrate the applicability of the model and its ability to estimate the error using
648 real snow depth data. Snow distributions in mountain environments have been shown to be
649 consistent intra- and inter-annually because the controlling processes are relatively consistent
650 during the season and from season to season. Such consistency suggests that the
651 correlation/covariance model should also be consistent, as well as the parameters of the model.
652 These parameters can be estimated via a dense survey either manually or with TLS of one or
653 more small plots of a size similar to the size that is aimed to be represented. These surveys would
654 not necessarily have to be repeated as the parameters and covariance models should be
655 preserved. Detailed surveys can be conducted under different conditions to characterize the range
656 of the correlation models and parameters (e.g., after a snow storm, or close to peak
657 accumulation). Also here, we should point out that although we show results for a wide range of
658 the exponential decay exponent values, we are finding that most of the values that we have
659 observed are in the lower range of those presented (e.g., $0.1-0.2 \text{ m}^{-1}$). Hence, the biases in the
660 estimated error and the survey design remain small.

661 Currently, remote sensing technologies (e.g., TLS, Airborne LiDAR, and ground penetrating
662 radar) are allowing for the characterization of snow cover properties at increasing resolutions in
663 both space and time. Such improvements can be utilized in the context presented here providing
664 information about the range of best fitting covariance/correlation models and parameters for

Ernesto 12/5/2015 11:28

Deleted: of this model

Ernesto 12/5/2015 11:29

Deleted: , which we have done

Ernesto 12/5/2015 11:31

Deleted: s

668 different conditions, supporting the application of methodologies such as the one presented here.
669 With such improvements, survey designs can be optimized such that estimation errors can be
670 explicitly addressed and accounted for, particularly when extrapolating a limited number of
671 measurements to estimate the spatial distribution of snow. Such applications will continue to be
672 relevant despite of the aforementioned improvements, as access to these technologies is limited
673 by their cost and the expertise that is required for their application.

674

675

676

7 Acknowledgements

677

Data for this article was obtained from NASA's Cold Land Processes experiment (CLPX),

678

available at http://nsidc.org/data/docs/daac/nsidc0157_clpx_lidar.

679

Figures

682 Figure 1. (a) Location of the Fraser and Rabbit Ears study areas in the state of Colorado (in
683 grey). (b) LIDAR Snow depth distributions on April 8, 2003, at the Saint Louis Creek Intensive
684 Study Area (ISA) and (c) on April 9 at the Rabbit Ears ISA.

685 Figure 2. (a) Sample normalized snow depth profile (mean = 0, standard deviation = 1) in a
686 forested environment from LIDAR (1-m resolution) at the Fraser – St. Louis Creek (FS)
687 intensive study area (ISA) of the Cold Land Processes eXperiment (CLPX) (Trujillo et al., 2007;
688 Cline et al., 2009). The profile is sampled with regular separations (spacing) of 5 m, 10 m, 25 m,
689 50 m, and 100 m (from top to bottom, respectively). (b) Average values within sampling
690 intervals (same as in (a)) versus point samples for normalized snow depth profiles in the FS ISA.
691 The red line is a linear regression fit, with slope β and r^2 as indicated in each plot. (c) Histograms
692 of the difference between the point and average values for each of the sampling intervals. The
693 vertical red line marks the mean difference.

694 Figure 3. (a) As Figure 2 but for an open and wind influenced environment at the Rabbit Ears
695 – Walton Creek (RW) ISA of the CLPX (Trujillo et al., 2007; Cline et al., 2009). (b) Average
696 values within sampling intervals (same as in (a)) versus point samples for normalized snow depth
697 profiles in the RW ISA. The red line is a linear regression fit, with slope β and r^2 as indicated in
698 each plot. (c) Histograms of the difference between the point and average values for each of the
699 sampling intervals. The vertical red line marks the mean difference.

700 Figure 4. Sub-interval standard deviation (a) and range (b) for varying interval lengths for
701 profiles of snow depth in a forested environment (FS) and an open and wind-influenced
702 environment (RW) in the Colorado Rocky Mountains (same regions as those in Figure 2 and
703 Figure 3). The mean standard deviation and mean range for the study areas are shown by the
704 solid lines, while the shaded areas cover the quantiles between 25% and 75% of the values for all
705 the intervals in these areas.

706 Figure 5. Survey designs for the sampling of a snow profile.

707 Figure 6. Comparison of the theoretical and sampled normalized squared error (σ_z^2/σ_p^2) for
708 the case of a single measurement along a profile section of length L , as in Figure 5a. The survey
709 case applied to profiles in FS and RW along the x and y directions. Solid lines are the theoretical
710 error using exponential decay exponents derived from the functions fitted to the sampled
711 correlation functions of the two surfaces in the x and y directions.

712 Figure 7. (a) Theoretical normalized squared error for a single measurement in the middle of a
713 section of length L , and for an exponential correlation function with a decay exponent, v . (b) and
714 (c) Comparison of the theoretical and sampled normalized squared error for the same survey case
715 applied to profiles in FS and RW along the x and y directions. Dashed lines are the theoretical
716 error from (7) using exponential decay exponents derived from the functions fitted to the
717 sampled correlation functions of the two surfaces in the x and y directions.

718 Figure 8. (a) and (b) Theoretical normalized squared error for the three-point pattern along a
719 profile section in Figure 5b, and for profile section lengths (L) of 1 (a) and 25 (b). Each of the

720 colored lines corresponds to a specific decay exponent, ν , and the black line marks the
721 theoretical solution for $a_{optimal}$. (c) Theoretical normalized error and $a_{optimal}$ for isolines of profile
722 section lengths (L) and exponential decay exponents (ν) for the three-point pattern along a profile
723 section of length L in Figure 5b.

724 Figure 9. Theoretical and sampled normalized squared error (σ_z^2/σ_p^2) for the three-point
725 pattern along a profile section in Figure 5b, and for profile section lengths (L) between 10 m and
726 80 m in FS and RW. The solid lines are the theoretical error from (8) using exponential decay
727 exponents derived from the functions fitted to the sampled correlation functions of the two
728 surfaces in the x and y directions, while the dots correspond to the sampled error for profiles in
729 FS (a-d) and RW (e-h).

730 Figure 10. Theoretical normalized squared error (σ_z^2/σ_p^2) for the N -point pattern along a
731 profile section in Figure 5c, and for profile section lengths (L) between 10 and 80 obtained from
732 (10).

733 Figure 11. Theoretical and sampled normalized squared error (σ_z^2/σ_p^2) for the N -point pattern
734 along a profile section in Figure 5c, and for profile section lengths (L) between 10 m and 80 m in
735 FS and RW. The solid point markers are the theoretical error from (10) using exponential decay
736 exponents derived from the functions fitted to the sampled correlograms of the two surfaces in
737 the x and y directions, while the circle markers with the dotted lines correspond to the sampled
738 error for profiles in FS (a-d) and RW (e-h).

739 Figure 12. Sample survey designs with (a) a 5-point pattern centered in the area, and (b) a
740 regularly spaced pattern. For the 5-point pattern, a can vary between 0 and $L/2$, while for the $N \times$
741 N points pattern, the separation between the measurements is determined by the number of
742 points.

743 Figure 13. (a) Theoretical normalized squared error (σ_z^2/σ_p^2) for the two-dimensional case
744 with a single measurement in the middle of a square area with side dimension L . (b) Theoretical
745 and sampled normalized squared error for the same two-dimensional survey applied to the snow
746 depth field in FS. The dashed line is the theoretical error derived for an exponential decay
747 exponent of 0.17 derived from the sampled correlation function of snow depth in FS, while the
748 solid line is the sampled normalized squared error for the snow cover in FS.

749 Figure 14. Theoretical normalized squared error (σ_z^2/σ_p^2) as a function of the distance a from
750 the center of the area for square areas of side dimensions (L) between 10 and 80. Each curve
751 corresponds to an exponential decay (ν) between 0.1 and 5.

752 Figure 15. Theoretical and sampled normalized squared error (σ_z^2/σ_p^2) for the 5-point pattern
753 in Figure 12a over square areas of side dimensions (L) between 10.7 m and 79.1 m. The
754 separation distance (a) is varied from the center outwards. The solid line is the theoretical error
755 derived for an exponential decay exponent of 0.17 derived from the sampled correlation function
756 of snow depth in FS, while the solid red point markers are the sampled normalized squared error
757 for the snow cover in FS.

758 Figure 16. Theoretical normalized squared error (σ_z^2/σ_p^2) for the N by N point pattern in
759 Figure 12b, and for areas of side dimension (L) between 10 and 80. The exponential exponent is
760 varied between 0.1 and 5.

761 Figure 17. Theoretical and sampled normalized squared error (σ_z^2/σ_p^2) for the N by N point
762 pattern in Figure 12b, and over square areas of side dimensions (L) between 10.7 m and 79.1 m.
763 The solid black point markers are the theoretical error for an exponential decay exponent of 0.17
764 derived from the sampled correlogram of snow depth in FS. The dotted red lines with circle
765 markers are the sampled normalized squared error for the snow cover in FS.

766

767

- 769 Blöschl, G.: Scaling issues in snow hydrology, *Hydrol. Processes*, 13(14-15), 2149-2175, 1999.
- 770 Chang, A. T. C., Kelly, R. E. J., Josberger, E. G., Armstrong, R. L., Foster, J. L., and Mognard,
771 N. M.: Analysis of ground-measured and passive-microwave-derived snow depth variations in
772 midwinter across the northern Great Plains, *J. Hydrometeor.*, 6(1), 20-33, doi: 10.1175/Jhm-
773 405.1, 2005.
- 774 Cline, D., Yueh, S., Chapman, B., Stankov, B., Gasiewski, A., Masters, D., Elder, K., Kelly, R.,
775 Painter, T. H., Miller, S., Katzberg, S., and Mahrt, L.: NASA Cold Land Processes Experiment
776 (CLPX 2002/03): Airborne Remote Sensing, *J. Hydrometeor.*, 10(1), 338-346, 2009.
- 777 Cressie, N.: *Statistics for spatial data*, 900 pp., John Wiley & Sons, Inc., USA, 1993.
- 778 Deems, J. S., Fassnacht, S. R., and Elder, K. J.: Interannual Consistency in Fractal Snow Depth
779 Patterns at Two Colorado Mountain Sites, *J. Hydrometeor.*, 9(5), 977-988, doi:
780 10.1175/2008jhm901.1, 2008.
- 781 Grünewald, T., and Lehning, M.: Are flat-field snow depth measurements representative? A
782 comparison of selected index sites with areal snow depth measurements at the small catchment
783 scale, *Hydrol. Processes*, doi: 10.1002/hyp.10295, 2014.
- 784 Helfrich, K., Schöber, J., Schneider, K., Sailer, R., and Kuhn, M.: Interannual persistence of the
785 seasonal snow cover in a glacierized catchment, *J. Glaciol.*, 60(223), 889-904, doi:
786 10.3189/2014JoG13J197, 2014.
- 787 Journel, A. G., and Huijbregts, C. J.: *Mining Geostatistics*, Academic Press, London, 1978.
- 788 Kronholm, K., and Birkeland, K. W.: Reliability of sampling designs for spatial snow surveys,
789 *Comput. Geosci.*, 33(9), 1097-1110, 2007.
- 790 Lopez-Moreno, J. I., Fassnacht, S. R., Begueria, S., and Latron, J. B. P.: Variability of snow
791 depth at the plot scale: implications for mean depth estimation and sampling strategies,
792 *Cryosphere*, 5(3), 617-629, 2011.
- 793 Matheron, G.: Application des méthodes statistiques à l'estimation des gisements, *Annales de*
794 *Mines, Dec*, 50-75, 1955.
- 795 Matheron, G.: Random functions, and their applications in geology, in *Geostatistics - A*
796 *colloquium*, edited by D. Merriam, pp. 79-87, Plenum Press, New York, 1970.
- 797 McCreight, J. L., Slater, A. G., Marshall, H. P., and Rajagopalan, B.: Inference and uncertainty
798 of snow depth spatial distribution at the kilometre scale in the Colorado Rocky Mountains: the
799 effects of sample size, random sampling, predictor quality, and validation procedures, *Hydrol.*
800 *Processes*, 28(3), 933-957, 2014.
- 801 Melvold, K., and Skaugen, T.: Multiscale spatial variability of lidar-derived and modeled snow
802 depth on Hardangervidda, Norway, *Ann. Glaciol.*, 54(62), 273-281, 2013.
- 803 Meromy, L., Molotch, N. P., Link, T. E., Fassnacht, S. R., and Rice, R.: Subgrid variability of
804 snow water equivalent at operational snow stations in the western USA, *Hydrol. Processes*,
805 27(17), 2383-2400, doi: 10.1002/Hyp.9355, 2013.

806 Mott, R., Schirmer, M., and Lehning, M.: Scaling properties of wind and snow depth distribution
807 in an Alpine catchment, *Journal of Geophysical Research: Atmospheres*, 116(D6), D06106, doi:
808 10.1029/2010jd014886, 2011.

809 Pomeroy, J. W., and Gray, D. M.: *Snow Accumulation, Relocation and Management (NHRI*
810 *Science Report No. 7)*, Environment Canada, Saskatoon, 1995.

811 Rice, R., and Bales, R. C.: Embedded-sensor network design for snow cover measurements
812 around snow pillow and snow course sites in the Sierra Nevada of California, *Water Resour.*
813 *Res.*, 46, W03537, doi: 10.1029/2008wr007318, 2010.

814 Rodríguez-Iturbe, I., and Mejía, J. M.: Design of Rainfall Networks in Time and Space, *Water*
815 *Resour. Res.*, 10(4), 713-728, 1974.

816 Schirmer, M., Wirz, V., Clifton, A., and Lehning, M.: Persistence in intra-annual snow depth
817 distribution: 1. Measurements and topographic control, *Water Resour. Res.*, 47(9), W09516, doi:
818 10.1029/2010wr009426, 2011.

819 Shea, C., and Jamieson, B.: Star: an efficient snow point-sampling method, *Ann. Glaciol.*,
820 51(54), 64-72, 2010.

821 Skoien, J. O., and Blöschl, G.: Sampling scale effects in random fields and implications for
822 environmental monitoring, *Environ. Monit. Assess.*, 114(1-3), 521-552, doi: Doi
823 10.1007/S10661-006-4939-Z, 2006.

824 Sturm, M., and Wagner, A. M.: Using repeated patterns in snow distribution modeling: An
825 Arctic example, *Water Resour. Res.*, 46, 2010.

826 Trujillo, E., Ramirez, J. A., and Elder, K. J.: Topographic, meteorologic, and canopy controls on
827 the scaling characteristics of the spatial distribution of snow depth fields, *Water Resour. Res.*, 43,
828 W07409, doi: 10.1029/2006WR005317, 2007.

829 Trujillo, E., Ramirez, J. A., and Elder, K. J.: Scaling properties and spatial organization of snow
830 depth fields in sub-alpine forest and alpine tundra, *Hydrol. Processes*, 23, 1575–1590, doi:
831 10.1002/hyp.7270, 2009.

832 Watson, F. G. R., Anderson, T. N., Newman, W. B., Alexander, S. E., and Garrott, R. A.:
833 Optimal sampling schemes for estimating mean snow water equivalents in stratified
834 heterogeneous landscapes, *J. Hydrol.*, 328(3-4), 432-452, doi: 10.1016/J.jhydrol.2005.12.032,
835 2006.

836 Yang, D. Q., and Woo, M. K.: Representativeness of local snow data for large scale hydrologic
837 investigations, *Hydrol. Processes*, 13(12-13), 1977-1988, doi: 10.1002/(Sici)1099-
838 1085(199909)13:12/13<1977::Aid-Hyp894>3.0.Co;2-B, 1999.

839

840